RSC Advances

PAPER

View Article Online
View Journal | View Issue

Cite this: *RSC Adv.*, 2019, **9**, 35336

Hybrid catalysts based on N-heterocyclic carbene anchored on hierarchical zeolites†

Enrica Gianotti, *[a] Ivana Miletto, [a] Chiara Ivaldi,[a] Geo Paul,[a] Leonardo Marchese, [a] Marta Meazza, [b] Ramon Rios [b] and Robert Raja [b]

Received 17th September 2019
Accepted 18th October 2019

DOI: 10.1039/c9ra07516j

rsc.li/rsc-advances

Hybrid materials have been synthesized by anchoring a N-heterocyclic carbene (NHC) precursor on different inorganic zeolitic supports with hierarchical porosity, in particular hierarchical HZSM-5 and SAPO-5. Hierarchical porous inorganic supports have been obtained both by top-down and bottom-up approaches and the role of hierarchical porosity has been evaluated. A detailed physico-chemical characterization has been performed on the organic–inorganic hybrids using a multi-technique approach (XRD, volumetric and thermogravimetric analysis, ssNMR and FTIR) in order to establish a structure–property relationship. The hybrids were tested in the benzoin condensation reaction of furfural, a base catalyzed reaction.

1. Introduction

Hybrids materials represent a new class of heterogeneous catalysts that combine the advantages of individual organic and inorganic components, allowing one to obtain solids with high mechanical, structural and hydrothermal stability together with the flexibility and functionality typical of organic molecules.[1–3] The nature of the organic–inorganic interface, including the types of organic–inorganic interactions, the hydrophobic or hydrophilic surface character and the type of bonds plays a strong role in controlling the properties (electrical, optical, mechanical, separation capacity, catalysis, sensing capability, and chemical and thermal stability) of the hybrids.[4–6] To be used as heterogeneous catalysts, the hybrids have to be synthesized by a robust immobilization method that prevents the active sites leaching in harsh reaction conditions and preserves the intrinsic high activity and selectivity of the organic moiety; for this reason, the organic part has to be covalently bound to the inorganic supports producing Class II hybrids.[7,8] Different inorganic architectures can be used as supports to immobilize organic moieties; in this work, hierarchical porous (HP) supports synthesized both by bottom-up and top-down approaches were developed to host the organic functionality. Hierarchical porous materials can be considered zeo-type systems possessing a bimodal pore size distribution, consisting of micropores and a secondary porosity, usually in the mesopores range.[9] The connectivity of the two sets of pores enhances the accessibility of the catalytic active sites and the mass transport of substrates avoiding coke deposition and catalyst deactivation.[10] Several strategies can be followed to synthesize hierarchical materials and can be classified as bottom-up and top-down approaches, depending on whether the production of the secondary porosity is induced during or after the zeolite crystallization.[11,12] Generally, top-down approaches involve post-synthetic modification, such as demetallation under acidic or basic conditions, to extract framework constituents whilst preserving crystallinity. On the contrary, bottom-up approach often uses sophisticated, but sacrificial, surfactants that guide, through the micelle formation, the mesopores network, together with the template to drive the formation of the microporous structure. The bottom-up approach is a facile procedure, being compatible with a 'one-pot' synthesis, and benefits from a high degree of structural control through the modification of the micellar structure.[12] Hierarchical HZSM-5 zeolite (HP-HZSM-5) prepared by top-down method[13] and hierarchical silicoaluminophosphate SAPO-5 (HP-SAPO-5) synthesized by bottom-up method[14] have been used as inorganic supports for anchoring N-heterocyclic carbene (NHC) precursor. Both inorganic frameworks possess Brønsted acid sites typical of their microporous counterparts. The use of such inorganic supports could be extremely advantageous in order to couple the acid strength of the inorganic part to the basic functionality of anchored NHC, producing a bifunctional acid–base hybrid heterogeneous catalyst for cascade reactions. Hierarchical SAPO-5 was synthesized by a new bottom-up approach using mesoporous SBA-15 containing Pluronic123 as source of silicon and mesoporogens,[14] while hierarchical HZSM-5 was obtained by desilication method in NaOH solution.[13] Both approaches used to produce hierarchical

[a]Department of Science and Technological Innovation, Università del Piemonte Orientale, V. T. Michel 11, I-15121 Alessandria, Italy. E-mail: enrica.gianotti@uniupo.it

[b]School of Chemistry, University of Southampton, University Road, Southampton, SO17 1BJ, UK

† Electronic supplementary information (ESI) available. See DOI: 10.1039/c9ra07516j

architectures induced the formation of surface silanol groups (Si–OH) in the mesopores[13,14] that are the *loci* for anchoring the NHC precursor and could, in principle, modify the Brønsted acidity of the inorganic frameworks. NHC are important class of organocatalysts that catalyze a variety of organic transformations,[15–17] such as C–C bond formation. NHC pre-catalyst derived from benzimidazolium salt has been grafted on different hierarchical supports to obtain a robust hybrid organic–inorganic heterogeneous catalysts.[18–20] The NHC catalytic function is generated during the catalytic reaction by *in situ* deprotonation of the benzimidazolium salt with a strong base.[18,21] The role of the inorganic supports, prepared with different methods, and the organic–inorganic interface have been investigated to establish structure–properties relationships by a detailed physico-chemical characterization using a multi techniques approach (XRD, volumetric and thermogravimetric analysis, ssNMR, FT-IR). Preliminary catalytic tests in benzoin condensation of furfural have been also performed to evaluate the catalytic activity of the NHC basic sites.

2. Results and discussion

The synthetic procedures, top-down or bottom-up, to obtain hierarchical zeo-type materials generally induce the formation of silanol groups in mesopores that can be used to anchor organic molecules; in this way organic–inorganic hybrid materials, belonging to Class II, are produced and due to the presence of a covalent bond between the inorganic and organic parts can be used as heterogeneous catalysts.

Silylated N-heterocyclic carbene (NHC) precursor, carrying a long chain (C_{12}) substituent at the N atom, was anchored on silanol groups (Si–OH) present in the mesopores of the calcined hierarchical HZSM-5 and SAPO-5 supports as represented in Scheme 1. The role of the long-chain alkyl is to avoid NHC deactivation by dimerization and to sterically protect the NHC catalytic site.[22] The acronyms of the hybrid catalysts, together with their elemental analysis and organic loadings are reported in Table 1. The organic loading is almost similar for both the hybrid materials.

In order to confirm phase purity, crystallinity and retention of the structural properties of the inorganic supports upon the carbene anchoring procedure, XRD analysis on hybrid catalysts has been performed. The XRD diffraction patterns of the NHC/HP-HZSM-5 and NHC/HP-SAPO-5 (Fig. S1 and S2 in the ESI†) showed the same diffraction peaks present before the NHC anchoring procedure confirming the retention of the structural properties of the supports. In addition, the MFI and AFI structures typical of ZSM-5 and SAPO-5 are evidenced in the hierarchical supports and hybrid catalysts.

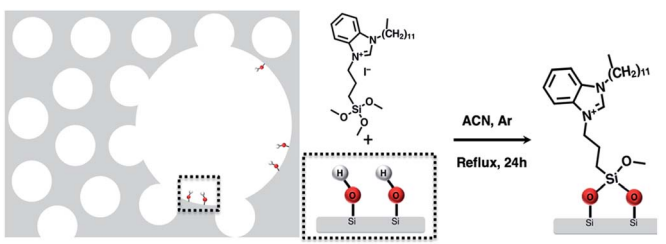

Scheme 1 Graphic representation of NHC precursor anchoring procedure on hierarchical supports.

Table 1 Acronyms, elemental analysis and organic loading of the hybrid catalysts

Acronyms of the hybrids	C%	H%	N%	Organic loading (mmol g^{-1})
NHC/HP-HZSM-5	9.15	1.55	0.56	0.20
NHC/HP-SAPO-5	7.61	1.55	0.62	0.25

Thermogravimetric analysis was performed in order to gain insight into the organic content and the thermal stability of the anchored NHC precursor on hierarchical supports (Fig. 1). The first weight loss observed in all materials at around 30–180 °C can be associated to the removal of physisorbed water and highlighted that the HP-SAPO-5 is a more hydrophilic support with respect to the HP-HZSM-5 due to the higher amount of physisorbed water. At higher temperatures, flat weight loss profiles of the hybrids changed into a rapidly declining profile corresponding to the decomposition of the organic NHC. The organic content, calculated from the weight loss in the 180–1000 °C range, due to the decomposition of the anchored NHC is reported in Table 2 and is in line with the data from elemental analysis. In addition, from the DTG curves, it is possible to observe that the temperature of weight loss due to the anchored NHC is around 270 °C for both hybrids.

N_2 adsorption/desorption at 77 K on both hierarchical supports revealed type-IV isotherms typical of mesoporous

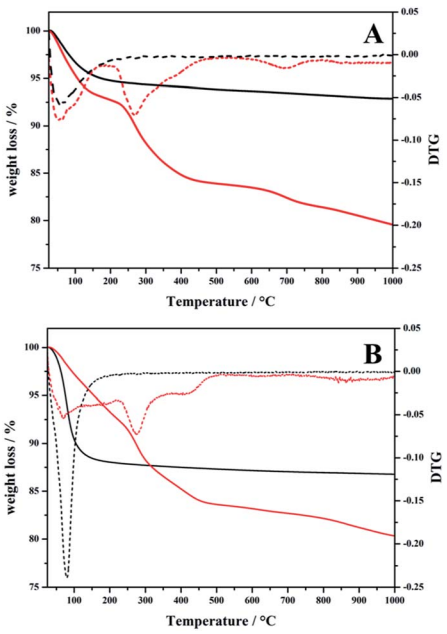

Fig. 1 TGA/DTG curves of (A) plain HP-HZSM-5 (black curves) and NHC/HP-HZSM-5 (red curves) and of (B) plain HP-SAPO-5 (black curves) and NHC/HP-SAPO-5 (red curves).

Table 2 Weight loss (%) due to water and organic content calculated from TGA analysis

Samples	Δwt% due to H_2O[a]	Δwt% due to NHC[b]
HP-HZSM-5	5	—
NHC/HP-HZSM-5	7	13.5
HP-SAPO-5	12	—
NHC/HP-SAPO-5	6	14

[a] Physisorbed H_2O calculated from 30 °C to 180 °C. [b] Calculated from 180 °C to 1000 °C.

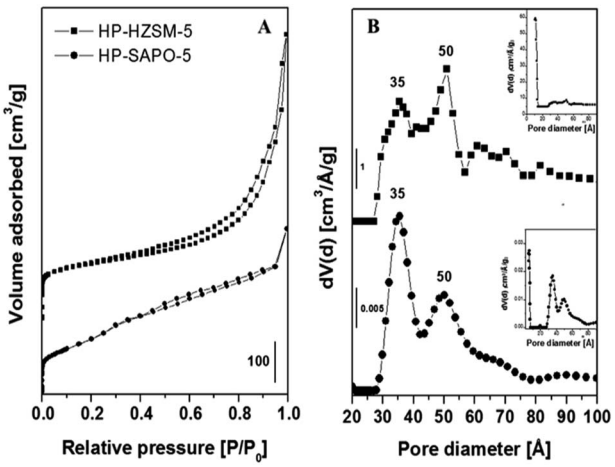

Fig. 2 (A): N_2 adsorption/desorption isotherms at 77 K of HP-HZSM-5 and HP-SAPO-5. (B): the pore size distribution in the mesopore range, with pore size distribution in the micropore (inset) and mesopore range.

materials (Fig. 2A), while microporous analogues have type-I isotherms.[13,23] Pore size distributions (Fig. 2B) were obtained by NLDFT (non-localized density functional theory) method by analyzing the desorption branch of the isotherms.[24,25] Hierarchical inorganic supports exhibited, a part of the micropores typical of the MFI and AFI structures, mesopores at 35 and 50 Å. Details of the specific surface area and pore volumes, determined by the NLDFT, are summarized in Table 3.

Volumetric data support the successful preparation of hierarchical inorganic supports and indicate the coexistence of multiple levels of porosity. HP-HZSM-5 showed a higher mesopore volume (V_{meso}) and total pore volume (V_{tot}) with respect HP-SAPO-5. Upon NHC anchoring on the hierarchical supports, the N_2 adsorption capacity decreases together with the specific surface area and pore volume (Fig. S3†), confirming that the NHC moiety is anchored inside the pores. Nevertheless, the textural properties of NHC/HP-HZSM-5 are less affected by the NHC presence with respect NHC/HP-SAPO-5 due to the different framework architectures and to the synthetic method used to prepare the hierarchical supports.

A combined study coupling FTIR and ssNMR spectroscopies has been performed to elucidate the interaction of the organic NHC moiety with the inorganic supports and to evidence the OH population before and after the organic grafting in order to understand the role of the hierarchical supports in stabilizing NHC molecules and the fraction of the OH involved in the NHC grafting.[26]

In order to establish if the Si–OH group in NHC/HP-HZSM-5 have been consumed upon NHC grafting and if the bridging Si–OH–Al groups (Brønsted acid sites, BAS) typical of the HZSM-5 and SAPO-5 frameworks have been retained after the grafting procedure, FT-IR spectra of NHC/HP-HZSM-5, NHC/HP-SAPO-5 and their inorganic analogue HP-HZSM-5 and HP-SAPO-5 were recorded (Fig. 3 and 4). All samples were treated 180 °C in vacuum to remove adsorbed water. In the spectra of plain HP-HZSM-5 (Fig. 3, black curve) and HP-SAPO-5 (Fig. 4, black curve), the signal at 3745 cm^{-1}, assigned to the O–H stretching mode of isolated Si–OH, disappeared upon NHC grafting (red curves), confirming that all the Si–OH anchoring sites have been consumed. The broad band at 3611 cm^{-1}, in the HP-HZSM-5 spectrum, is assigned to O–H stretching mode of Brønsted acid sites belonging to zeolite framework.[13] In contrast, HP-SAPO-5 exhibits two well separated bands at 3630 and 3515 cm^{-1} associated to Brønsted acid sites in different position inside the AFI framework.[27] The high frequency band is due to sites located in the 12-ring channels, while the band at 3515 cm^{-1} can be attributed to bridging OH located in the 6-

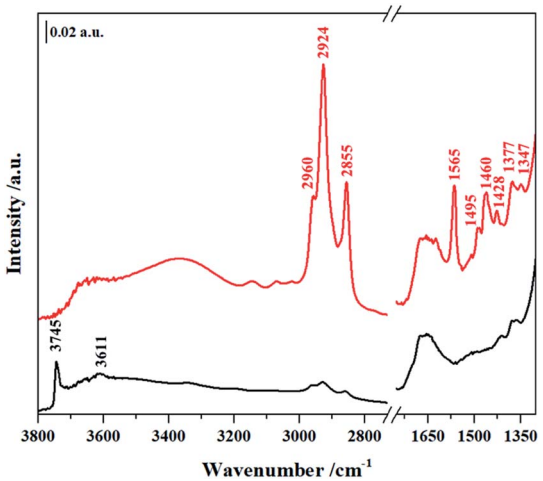

Fig. 3 FTIR spectra of plain HP-HZSM-5 (black curve) and NHC/HP-HZSM-5 (red curve) outgassed at 180 °C.

Table 3 Textural properties of the HP-HZSM-5 and HP-SAPO-5

Samples	S_{BET} ($m^2\ g^{-1}$)	S_{DFT} ($m^2\ g^{-1}$)	S_{micro} ($m^2\ g^{-1}$)	S_{meso} ($m^2\ g^{-1}$)	$V_{tot\ DFT}$ ($cm^3\ g^{-1}$)	V_{micro} ($cm^3\ g^{-1}$)	V_{meso} ($cm^3\ g^{-1}$)
HP-SAPO-5	573	508	215	293	0.49	0.05	0.44
HP-HZSM-5	500	731	516	215	0.80	0.10	0.70

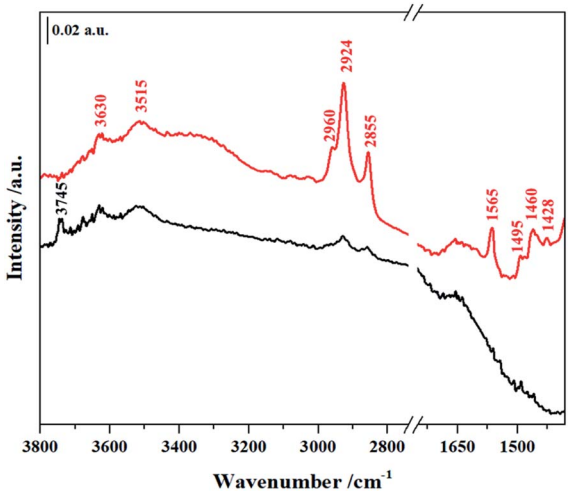

Fig. 4 FTIR spectra of plain HP-SAPO-5 (black curve) and NHC/HP-SAPO-5 (red curve) outgassed at 180 °C.

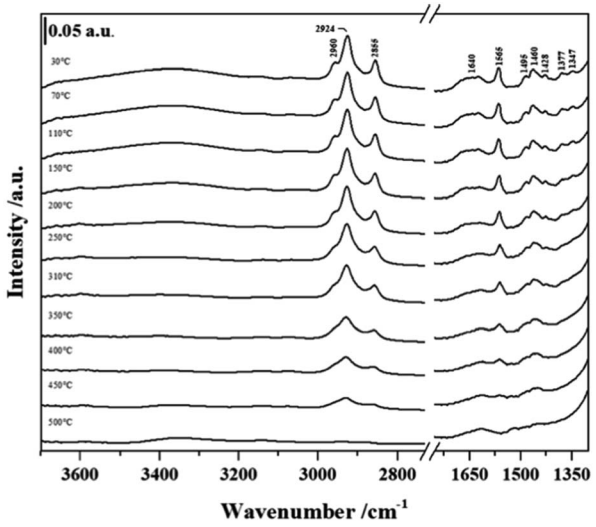

Fig. 5 Variable temperature FTIR spectra of NHC/HP-HZSM-5.

ring channels.[28,29] The signals of Brønsted acid sites are still visible in the spectra of NHC/HP-HZSM-5 and NHC/HP-SAPO-5, meaning that these acid groups are not involved in the NHC grafting. At lower frequencies, the signals, present only in the NHC-hybrids spectra (Fig. 3 and 4, red curves), are due to the organic component of the hybrids. In particular, absorptions arising from asymmetric and symmetric C–H stretching modes in the aromatic ring occurs in the region of 3150–3000 cm^{-1}. In the region 3000–2800 cm^{-1}, C–H stretching signals of aliphatic compounds are observed: at 2960 cm^{-1} and 2924 cm^{-1} are visible the asymmetric stretching vibrations of $-CH_3$ and $-CH_2$ groups respectively, while the symmetric stretching modes are observed at 2855 cm^{-1} for both $-CH_2$ and $-CH_3$. In the region between 1650–1400 cm^{-1}, the C–C ring stretching modes are present. These signals are overlapped with the $-CH_2$ and $-CH_3$ bending vibrations of aliphatic compounds (1460–1350 cm^{-1}). The C–N stretching mode characteristic of the imidazole ring is observed at 1565 cm^{-1}.[19,30]

The thermal stability of NHC grafted on the different hierarchical supports was investigated by FTIR spectroscopy experiments carried out at different outgassing temperatures (Fig. 5 and 6). The FTIR signals due to C–H stretching modes (3050–2800 cm^{-1}) and C–C ring modes (1650–1400 cm^{-1}) of NHC anchored in the different hybrids upon outgassing at increasing temperature decreased in intensity together with the band due to the C–N stretching mode characteristic of the imidazole ring at 1565 cm^{-1}. By monitoring this signal, it is possible to determine the organic counterpart stability of the grafted compound during the thermal treatment. This signal decreases significantly in intensity at 250 °C and totally disappears at 400 °C.

Together with FTIR spectra, ^{1}H MAS NMR spectroscopy provided direct information about the different proton sites present in the hierarchical inorganic supports (Fig. 7). The proton spectra of calcined and dehydrated hierarchical supports consist of contributions from isolated external silanols (1.8–2.0 ppm), hydroxyl units bound to Lewis acid sites (LAS) and extra framework aluminum species (EFAl) through hydrogen bonding (2.4–2.8 ppm), Brønsted acid sites (3.8–5.0 ppm) and hydrogen-bonded hydroxyls (5.8 ppm).[31–33] In the case of HP-SAPO-5, two different signals, due to Brønsted acid sites, are evidenced in agreement with the FTIR data. Quantitative representations of various protonic species are shown in Table 4. Furthermore, ^{27}Al TRAPDOR NMR spectra were recorded to separate contribution from silanols and Brønsted acid sites (Fig. S4†). The ^{1}H/^{27}Al TRAPDOR NMR method allows to differentiate protons that are dipolar coupled to nearby Al atoms, such as Brønsted and Lewis acid sites as well as Al–OH, from all other protons.[34] Two ^{1}H spin-echo NMR spectra were collected, without and with ^{27}Al irradiation. While the former displays all the protons in the sample, a difference spectrum will show only protons in close vicinity to ^{27}Al. These data clearly demonstrate that HP-HZSM-5 has a higher amount of

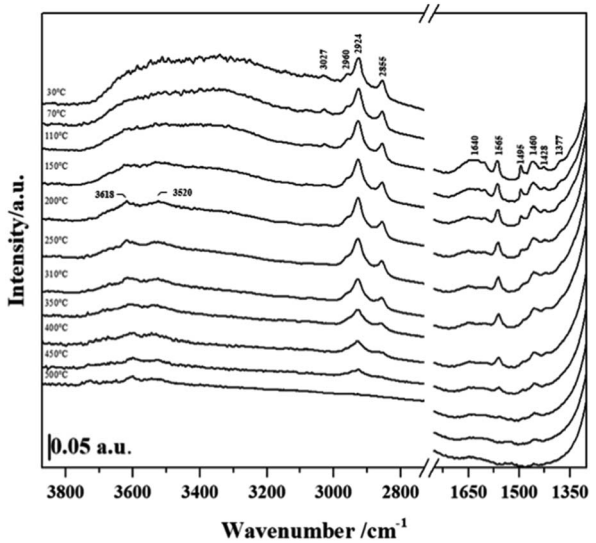

Fig. 6 Variable temperature FTIR spectra of NHC/HP-SAPO-5.

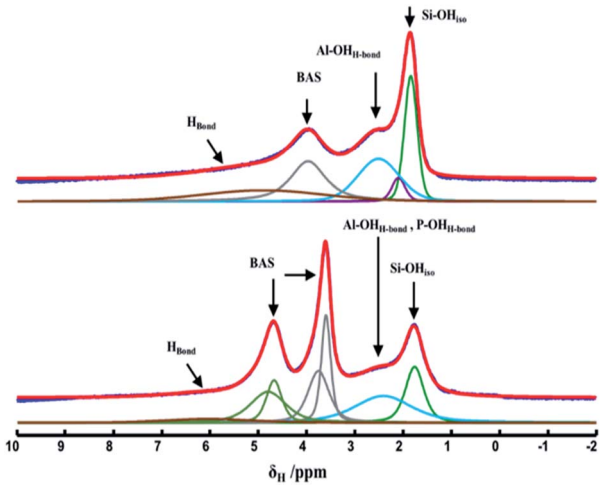

Fig. 7 ^{1}H MAS NMR spectra of calcined and dehydrated HP-HZSM-5 (top) and calcined HP-SAPO-5 (bottom) recorded at a MAS rate of 15 kHz. Each spectrum includes experimental and its fitted spectrum with individual contribution from each ^{1}H sites.

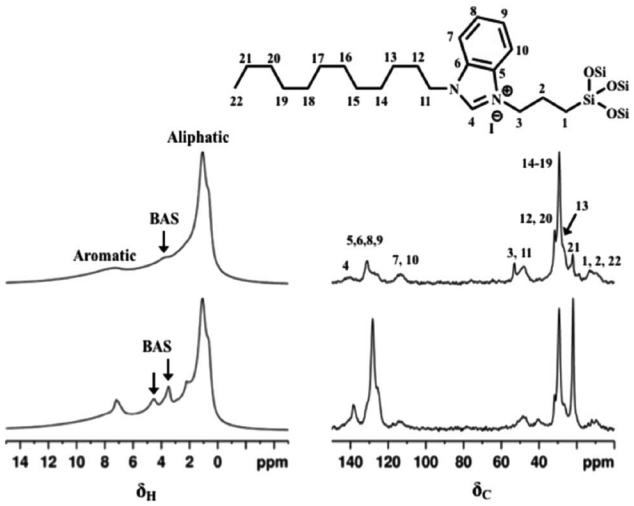

Fig. 8 ^{1}H MAS NMR (left panel) and ^{13}C CPMAS NMR spectra (right panel) of NHC/HP-HZSM-5 (top) and NH/HP-SAPO-5 (bottom). ^{1}H MAS NMR spectra were recorded using a MAS rate of 15 kHz and the ^{13}C CPMAS NMR spectra were recorded using a MAS rate of 11 kHz and CP contact time of 2 ms.

available Si–OH groups with respect HP-SAPO-5 and low amount of Brønsted acid sites.

Upon NHC grafting, the peak at 1.8 ppm due to Si–OH is not visible while the signals of the Brønsted acid site of the inorganic frameworks are still present in the ^{1}H MAS NMR spectra for both hybrids (Fig. 8, left panel), confirming that silanols are used to anchor the NHC precursor and the Brønsted acid sites are not affected by its presence. The signals in the 0–3 ppm range due to the aliphatic chain on the N-pyrrolic ring and a broad signal from 6.5 to 11 ppm due to aromatic protons are also visible. The imidazole proton, the active site of NHC, which in the liquid phase is at 11 ppm, is also present in this range. The successful grafting of the silylated NHC moiety was additionally verified by solid-state ^{13}C CPMAS NMR (Fig. 8, right panel) and the signals due to C in aliphatic chains are in the 20–35 ppm range. Terminal methyl and methylene carbons as well as the propylic linker carbons resonate in the 5–15 ppm range. At around 50 ppm the signal of the two N–CH_2 groups is visible, while the signals of the carbon atoms of the benzimidazole moiety are in the 110–140 ppm range.

The chemical environment of the framework atoms in hierarchical supports and NHC-containing hybrids was evaluated by ^{27}Al, ^{31}P and ^{29}Si MAS NMR (Fig. S5 and S6†). The ^{29}Si CP MAS NMR spectra of NHC/HP-ZSM-5 (Fig. S5†) exhibit signals due to Q sites −112 (Q^4(0Al)), −105 (Q^4(1Al)), −100 (Q^3(0Al)) and −90 (Q^2(0Al) ppm) owing to tetrahedral framework Si coordinated to four, three, and two Si atoms and signals due to T sites at −65 ppm (T^3, [RSi(OSi)$_3$]) and at −57 ppm (T^2, [RSi(OSi)$_2$OH]), confirming the success of the grafting procedure. The ^{27}Al MAS NMR spectra evidenced the presence of tetrahedrally coordinated Al (Al^{IV}, signal at *ca.* 54 ppm). Between 1–9 ppm a broad signal is visible due to six-coordinated Al sites (Al^{VI}), the presence of these octahedral Al sites is due to the desilication process to obtain the hierarchical framework.[13] In the case of HP-SAPO-5, the ^{31}P MAS NMR spectra are also recorded (Fig. S6†). The ^{29}Si CP MAS NMR spectra of NHC/HP-SAPO-5 reveals Q and T sites, the relative intensity of the Q sites is different from that of HP-HZSM-5, revealing a different degree of defectivity. The ^{27}Al MAS NMR spectra evidenced the presence of tetrahedrally coordinated Al (Al(OP)$_4$, signal at *ca.* 37 ppm) and no signal due to six-coordinated Al sites are present. Finally, the ^{31}P MAS NMR spectra exhibit a single peak at −30.5 ppm assigned to tetrahedrally-coordinated P atoms.

Table 4 Proton population distribution obtained from the ^{1}H MAS NMR spectra of calcined and dehydrated HP-HZSM-5 and HP-SAPO-5. FTIR frequencies of the corresponding OH groups are also reported

			^{1}H species (%)	
ν_{OH}/cm^{-1}	^{1}H chemical shift (δ)/ppm	Assignments	HP-HZSM-5	HP-SAPO-5
3745	1.8–2.1	Isolated Si–OH	29	15
	2.4–2.5	OH bound to lewis acid and EFAl species (LAS)	26	22
3618–3615	3.8	Brønsted acid sites (BAS)	26	32
3520	4.8	Brønsted acid sites (BAS) in small cages	—	26
≈3500	5.8	H-bonded species	19	5

Since both ^{27}Al and ^{31}P MAS NMR spectra have only a single resonance, it is possible to confirm strictly alternation of Al and P atoms at the T-positions of the SAPO-5 framework.

NHC based hybrid catalysts were tested in the reaction of self-condensation of furfural (Scheme 2), a carbene catalyzed reaction at room temperature.[35] The reaction starts with the deprotonation of the benzimidazole moiety by the organic base (1,8-diazabicyclo[5.4.0]undec-7-ene, DBU), forming the active carbene catalyst. The hybrid catalyst reacts with one molecule of furfural, forming the Breslow intermediate, which undergoes a nucleophilic attack to another non-activated molecule of furfural, with formation of the furoin as final product. We envisage the solid acid sites present on the hierarchical HP-ZSM-5 and HP-SAPO-5 supports can coordinate with the substrate (*via* the carbonyl group), thereby increasing their electrophilicity, which favours the nucleophilic attack of the NHC. Preliminary results showed better catalytic performances of NHC/HP-HZSM-5 hybrid with respect NHC/HP-SAPO-5 (Fig. 9). In fact, almost 98% yield was reached when NHC/HP-ZSM-5 hybrid is used as heterogeneous catalyst. Both hybrid catalysts can be recycled and reused with the NHC/HP-HZSM-5 showing a more sustained performance post recycling.

Control experiments with hierarchical HP-ZSM-5 and HP-SAPO-5 (without the anchored NHC) have been carried out and we did not observe any reactivity with these catalysts. This further emphasises the role of the anchored N-heterocyclic carbene in the catalytic process.

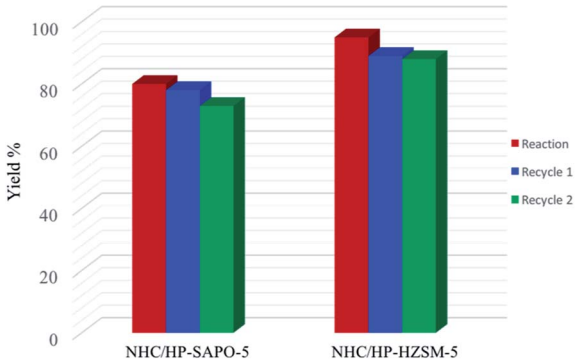

Fig. 9 Catalytic activity and recycling tests of NHC-based hybrids in benzoin condensation reaction. The yield (%) is reported after 20 h of reaction.

3. Experimental

3.1. Materials

3.1.1. Synthesis of hierarchical HZSM-5 (HP-HZSM-5). Commercial NH_4–ZSM-5 zeolite was supplied by Zeolyst International with $SiO_2/Al_2O_3 = 80$ (CBV 8014). After conversion to the protonated forms, through calcination at 550 °C for 16 h under airflow, the H-ZSM-5 was treated in a 0.2 M NaOH solution (solid/liquid ratio = 22 g L^{-1}) for 3 h. The basic solution was heated in a glass reactor at 65 °C, under reflux; than the zeolite was added; the flask was cooled down in an ice bath after 3 h and washed with deionized water until pH 7; the material obtained was dried overnight, at 60 °C. To convert the hierarchical Na–ZSM-5 into the acidic forms, an ion exchange with a NH_4NO_3 solution at 80 °C was performed (solid/liquid ratio = 6.7 g L^{-1}) and finally, the material was calcined in air at 600 °C for 16 h.[13]

3.1.2. Synthesis of hierarchical SAPO-5 (HP-SAPO-5). HP-SAPO-5 has been synthesized using Pluronic123 encapsulated within ordered mesoporous silica SBA-15, which serves both as silicon source and as mesoporogen. Aluminium isopropoxide (7.00 g, Sigma Aldrich) was added slowly to deionized water (10 ml) under stirring. Then, triethylamine (TEA) (2.76 ml, Sigma Aldrich) was added and the mixture was stirred for 1 h. Pluronic123-containing SBA-15 (1.5 g) was slowly added with 5 ml of deionized water and the mixture was further stirred for 2 h. Phosphoric acid (2.18 mL, 85 wt% in H_2O, Sigma Aldrich) was added dropwise under stirring. The gel was vigorously stirred for 30 min to produce a white gel with the following composition: 1.0 Al : 0.93 P : 0.58 Si : 0.068 Pluronic123 : 0.58 TEA : 28 H_2O.

The gel was transferred to a Teflon-lined stainless-steel autoclave and crystallized at 473 K for 60 h under autogenous pressure. The solid product from autoclave was then recovered by filtration and washed with water. The as-prepared product was dried in air at 373 K and calcined in a tube furnace under air flow at 873 K for 16 h to remove organic surfactant and micropore template, producing a white crystalline solid.[14]

3.1.3. Preparation of the N-heterocyclic carbene precursor. The first step in the preparation of NHC precursor was the 1-alkylation of benzimidazole (Scheme 3).

Benzimidazole (8.46 mmol) was added slowly to a suspension of NaH (1 equiv.) in THF (6 ml) under argon at 0 °C and the solution was left stirring for 30 min at room temperature. Then, dodecylbromide (8.46 mmol) was added dropwise and left to reflux for 24 h. Then the solution was filtered and washed with CH_2Cl_2 over a pad of celite. Then the solvent was evaporated and the product was purified *via* chromatographic column. Yield: 97%. ^{1}H-NMR ($CDCl_3$, 500 MHz, ppm): 0.90 (t, –CH_2–$\underline{CH_3}$), 1.25–1.35 (m, N–CH_2–CH_2–$(\underline{CH_2})_9$–CH_3), 1.89 (q, N–CH_2–$\underline{CH_2}$–$(CH_2)_9$–CH_3), 4.17 (t, N–$\underline{CH_2}$–CH_2–$(CH_2)_9$–CH_3), 7.83 (m, Ar), 7.90 (s, N–$\underline{CH}$–N). ^{13}C-NMR ($CDCl_3$, 125 MHz, ppm): 14 (–N–$(CH_2)_{11}$–$\underline{CH_3}$), 22 (–N–$(CH_2)_{10}$–$\underline{CH_2}$–CH_3), 26.8, 29.1, 29.3, 29.4, 29.58, 29.6, 29.85 (aliphatic chain), 31.9 (N–CH_2–$\underline{CH_2}$–$(CH_2)_9$), 45.12 (N–$\underline{CH_2}$–CH_2–$(CH_2)_9$), 109.65, 120.38,

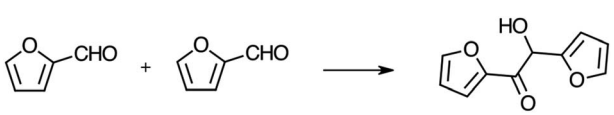

Scheme 2 Graphic representation of benzoin condensation reaction.

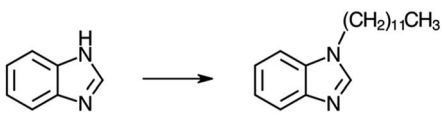

Scheme 3 Graphic representation of 1-alkylation of benzimidazole.

121.98, 122.75, 133.84, 143.90 (aromatic except N–CH–N), 142.93 (N–*CH*–N).

After the alkylation of benzimidazole, the carbene precursor was silylated; this procedure is necessary to have siloxane groups able to anchor to the Si–OH of the inorganic supports. The NHC-silylated precursor was prepared in accordance to previously reported literature data (Scheme 4).[22]

The 1-alkylated benzimidazole (8.20 mmol) was dissolved in ACN solvent (12 ml), then 1-iodo-3(methoxysilyl)propane (12.3 mmol) was added and left stirring for 24 h under argon. Once the reaction was finished, the product was washed with anhydrous pentane. Yield: 95%. ^{1}H-NMR ($CDCl_3$, 500 MHz, ppm): 0.80 (t, –CH_2–$\underline{CH_3}$), 0.699 (O–Si–$\underline{CH_2}$–CH_2), 1.11–1.41 (m, N–CH_2–CH_2–$\underline{(CH_2)_9}$–CH_3), 2 (q, N^+–CH_2–$\underline{CH_2}$–CH_2–Si), 2.11 (q, N–CH_2–$\underline{CH_2}$–$\underline{(CH_2)_9}$–CH_3), 3.55 (O–$\underline{CH_3}$), 4.53 (t, N–$\underline{CH_2}$–CH_2–$(CH_2)_9$–CH_3), 4.58 (t, N^+–$\underline{CH_2}$–CH_2–CH_2–Si), 7.58–7.69 (m, Ar), 11.1 (s, N–$\underline{CH}$–N). ^{13}C-NMR ($CDCl_3$, 125 MHz, ppm): 14 (–N–$(CH_2)_{11}$–$\underline{CH_3}$), 22.3, 22.7, 23.3, 26.6, 29, 29.31, 29.37, 29.49, 29.5, 29.57, 31.9, 34.1 (aliphatic chain), 50.8 (CH_2–Si–O–$\underline{(CH_3)_3}$), 113, 113.24, 127.21, 127.24 (aromatic except N–CH–N), 141.94 (N–$\underline{CH}$–N).

3.1.4. Preparation of the N-heterocyclic hybrid materials. The hybrid materials were prepared by post-synthesis grafting with silylated NHC precursor. 0.5 mmol of silylated carbene precursor was added to 10 ml of anhydrous toluene, then 0.500 g of the hierarchical inorganic supports (HP-HZSM-5 and HP-SAPO-5) were stirred under argon reflux for 24 h. The reaction solution was filtered and washed with toluene. The obtained yellow solids were cured in air at 80 °C overnight.

3.2. Methods

Elemental analysis was collected on Thermo Scientific Flash EA 1112 Series (CHNS), with sulfanilamide used as the standard for calibration purposes. To determine the amounts present a sample of known mass is burned at 900 °C within a high oxygen atmosphere in order to produce the combustion products of CO_2, H_2O, NO or NO_2, and SO_2. The combustion products separated in by gas chromatography before entering a thermal conductively detector which measures the amount of each species, by changes in the thermal conductivity of the column output with respect to a reference flow of carrier gas (He or Ar). The thermal conductively will be reduced when an analyte passes through the gas flow and so can be accordingly detected with the use of a reference material and a calibration.

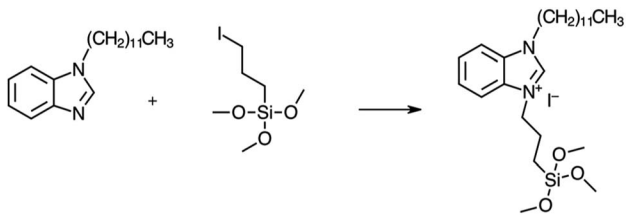

Scheme 4 Graphic representation of the NHC silylation reaction.

X-Ray powder diffraction (XRD) patterns were obtained using an ARL XTRA48 diffractometer with Cu Kα radiation (λ = 1.54062 Å).

N_2 physisorption measurements were carried out at 77 K in the relative pressure range from 1×10^{-6} to 1 P/P_0 by using a Quantachrome Autosorb1MP/TCD instrument. Prior to the analysis, the hierarchical supports were outgassed at 423 K for 3 h (residual pressure lower than 10^{-6} torr). Specific surface areas were determined using the Brunauer–Emmett–Teller equation, in the relative pressure range from 0.01 to 0.1 P/P_0. The desorption branch of the N_2 physisorption isotherm was analyzed by means of the NLDFT (non-localized density functional theory) method, to obtain the pore size distribution of the materials.

Thermogravimetric analyses were carried out on a Mettler TGA/SDTA 851e instrument, in nitrogen. The samples were heated from 30 to 1000 °C at a heating rate of 20°C min^{-1} under a gas flow rate of 60 ml min^{-1}.

FTIR spectra of self-supporting pellets at variable temperature were collected under vacuum conditions (residual pressure $< 10^{-4}$ mbar) using a Bruker Equinox 55 spectrometer equipped with a pyroelectric detector (DTGS type) with a resolution of 4 cm^{-1}. FTIR spectra were normalized with respect the pellet weight.

^{1}H-NMR and ^{13}C-NMR were recorded with a Bruker DPX400 NMR. Chemical shifts (δ) are reported in ppm relative to residual solvent signals ($CHCl_3$, 7.26 ppm for ^{1}H NMR; $CDCl_3$, 77.15 ppm for ^{13}C NMR).

Solid-state NMR spectra were acquired on a Bruker Avance III 500 spectrometer and a wide bore 11.7 Tesla magnet with operational frequencies for ^{1}H, ^{29}Si, ^{27}Al, ^{31}P and ^{13}C of 500.13, 99.35, 130.32, 202.45 and 125.77 MHz, respectively. A 4 mm triple resonance probe (in double resonance mode) with MAS was employed in all the experiments. The samples were packed on a Zirconia rotor and spun at a MAS rate between 10 and 15 kHz. The magnitude of radio frequency (RF) field was 100, 83, 42 kHz, for ^{1}H, ^{31}P and ^{29}Si, respectively, while a $\pi/12$ pulse was used for the ^{27}Al MAS experiment. The relaxation delay between accumulations was 5, 30, 60, 1 s for ^{1}H, ^{31}P, 29Si and ^{27}Al, respectively. For the ^{13}C and ^{29}Si Cross Polarization (CP) MAS experiments, the RF fields of 55 and 28 kHz were used for initial proton excitation and decoupling, respectively. During the CP period the ^{1}H RF field was ramped using 100 increments, whereas the ^{13}C/^{29}Si RF fields were maintained at a constant level. During the acquisition, the protons are decoupled from the carbons/silicons by using a two-pulse phase-modulated (TPPM) decoupling scheme. A moderate ramped RF field of 62 kHz was used for spin locking, while the carbon/silicon RF field was matched to obtain optimal signal and the CP contact time of 2 ms were used. All chemical shifts are reported using δ scale and are externally referenced to TMS for ^{1}H, ^{13}C and ^{29}Si, 1 M solution of $AlCl_3$ for ^{27}Al and ammonium dihydrogen phosphate for ^{31}P.

3.3. Catalysis

To a screw cap vial flushed with argon were added in this sequence: heterogeneous hybrid catalyst (0.02 mmol), anhydrous

dimethylformamide (0.4 mL), furfural (0.2 mmol) and DBU (0.6 mmol). In the vial was bubbled argon, then the vial was closed and left at room temperature for 20 h. To regenerate the hybrid catalysts, a HCl solution (0.4 μmol of HCl 37%) was added. The crude mixture was filtered to recover the catalysts and the catalysts were washed with methanol, dried under vacuum and reused in the next reaction. The conversion was checked by ^{1}H-NMR.

4. Conclusions

N-heterocyclic carbene (NHC) pre-catalyst has been anchored on different inorganic supports with hierarchical porosity, in particular hierarchical HZSM-5 and SAPO-5, to obtain organic–inorganic hybrid catalysts. The hierarchical inorganic supports have been synthesized following two different procedures: HP-HZSM-5 was produced using a top-down approach while HP-SAPO-5 using a bottom-up approach. The physico-chemical characterization of the inorganic supports has revealed that both supports have Si–OH groups with different abundance that have been used for anchoring NHC moieties, leaving available the Brønsted acid sites, typical of the inorganic zeolitic framework. The NHC hybrids can catalyze, in the presence of a suitable base, the self-coupling reaction of furfural. Good catalytic activity and recyclability has been reached for both hybrids, nevertheless the superior performances observed for NHC/HP-HZSM-5 hybrid can be due to the role of the inorganic hierarchical support in the dispersion of the NHC precursor. In fact, the top-down method used to synthesize HP-HZSM-5 induced the formation of a high fraction of silanols and high mesopores volumes that are less affected by the presence of the organic NHC inside the channels. Moreover, the concomitant presence of the Brønsted acid sites in the inorganic framework that are not affected by the presence of the organic base together with the anchored basic NHC functionality makes these systems extremely interesting as bifunctional hybrids to catalyze tandem reactions.

Conflicts of interest

There are no conflicts to declare.

Acknowledgements

The project leading to these results has received funding from the European Union's Horizon 2020 research and innovation pro-gram under grant agreement N. 720783—MULTI2HYCAT. L. Guarnieri is kindly acknowledged for experimental contribution.

References

1 A. P. Wight and M. E. Davis, *Chem. Rev.*, 2002, **102**, 3589–3614.
2 F. Hoffmann, M. Cornelius, J. Morell and M. Fröba, *Angew. Chem., Int. Ed.*, 2006, **45**, 3216–3251.
3 U. Díaz and A. Corma, *Chem.–Eur. J.*, 2018, **24**, 1–16.
4 S. H. Mir, L. A. Nagahara, T. Thundat, P. Mokarian-Tabari, H. Furukawa and A. Khosla, *J. Electrochem. Soc.*, 2018, **165**(8), B3137–B3156.
5 P. Judeinstein and C. Sanchez, *J. Mater. Chem.*, 1996, **6**(4), 511–525.
6 C. Sanchez, B. Juliàn, P. Belleville and M. Popall, *J. Mater. Chem.*, 2005, **15**, 3559–3592.
7 U. Díaz, D. Brunel and A. Corma, *Chem. Soc. Rev.*, 2013, **42**, 4083–4097.
8 R. Ye, J. Zhao, B. B. Wickemeyer, F. Dean Toste and G. A. Somorjai, *Nat. Catal.*, 2018, **1**, 318–325.
9 M. Hartmann, A. Gonche Machoke and W. Schwieger, *Chem. Soc. Rev.*, 2016, **45**, 3313–3330.
10 M. Milina, S. Mitchell, D. Cooke, P. Crivelli and J. Pérez-Ramírez, *Angew. Chem., Int. Ed.*, 2015, **54**, 1591–1594.
11 X.-Y. Yang, L.-H. Chen, Y. Li, J. C. Rooke, C. Sanchez and B.-L. Su, *Chem. Soc. Rev.*, 2017, **46**, 481–558.
12 D. P. Serrano, J. M. Escola and P. Pizarro, *Chem. Soc. Rev.*, 2013, **42**, 4004–4035.
13 A. Erigoni, S. H. Newland, G. Paul, L. Marchese, R. Raja and E. Gianotti, *ChemCatChem*, 2016, **8**, 3161–3169.
14 I. Miletto, G. Paul, S. Chapman, G. Gatti, L. Marchese, R. Raja and E. Gianotti, *Chem.–Eur. J.*, 2017, **23**, 9952–9961.
15 M. N. Hopkinson, C. Richter, C. M. Schedler and F. Glorius, *Nature*, 2014, **510**, 485–496.
16 D. Enders, O. Niemeier and A. Henseler, *Chem. Rev.*, 2007, **107**, 5606–5655.
17 P. de Fremont, N. Marion and S. P. Nolan, *Coord. Chem. Rev.*, 2009, **253**, 862–892.
18 K. V. S. Ranganath, S. Onitsuka, A. Kiran Kumar and J. Inanaga, *Catal. Sci. Technol.*, 2013, **3**, 2161–2181.
19 Z. Zhou, Q. Meng, A. Seifert, A. Wagener, Y. Sun, S. Ernst and W. Thiel, *Microporous Mesoporous Mater.*, 2009, **121**, 145–151.
20 R. Zhong, A. C. Lindhorst, F. J. Groche and F. E. Kühn, *Chem. Rev.*, 2017, **117**, 1970–2058.
21 L. Benhamou, E. Chardon, G. Lavigne, S. Bellemin-Laponnaz and V. César, *Chem. Rev.*, 2011, **111**, 2705–2733.
22 L. Wang and E. Y.-X. Chen, *ACS Catal.*, 2015, **5**, 6907–6917.
23 B. Boddenberg, V. R. Rani and R. Grosse, *Langmuir*, 2004, **20**, 10962–10969.
24 M. Thommes, S. Mitchell and J. Peŕez-Ramírez, *J. Phys. Chem. C*, 2012, **C116**, 18816–18823.
25 M. Thommes and K. A. Cychosz, *Adsorption*, 2014, **20**, 233–250.
26 G. Paul, C. Bisio, I. Braschi, M. Cossi, G. Gatti, E. Gianotti and L. Marchese, *Chem. Soc. Rev.*, 2018, **47**, 5684–5739.
27 M. E. Potter, M. E. Cholerton, J. Kezina, R. Bounds, M. Carravetta, M. Manzoli, E. Gianotti, M. Lefenfeld and R. Raja, *ACS Catal.*, 2014, **4**, 4161–4169.
28 S. I. Lee and H. Chon, *J. Chem. Soc., Faraday Trans.*, 1993, **93**, 1855–1860.
29 G. Müller, J. Bodis, G. Eder-Mirth, J. Kornatowski and J. A. Lercher, *J. Mol. Struct.*, 1997, **410–411**, 173–178.
30 N. B. Colthup, in *An introduction to infrared and Raman spectroscopy*, ed. L. H. Daly and S. E. Wiberlwy, Academic Press, Boston, USA, 1990.

31 Y. Jiang, J. Huang, W. Dai and M. Hunger, *Solid State Nucl. Magn. Reson.*, 2011, **39**, 116–141.
32 M. Hunger, S. Ernst, S. Steuernagel and J. Weitkamp, *Microporous Mater.*, 1996, **6**, 349–353.
33 E. J. M. Hensen, D. G. Poduval, V. Degirmenci, D. A. J. M. Ligthart, W. Chen, F. Mauge, M. S. Rigutto and J. A. R. van Veen, *J. Phys. Chem. C*, 2012, **116**, 21416–21429.
34 C. P. Grey and A. J. Vega, *J. Am. Chem. Soc.*, 1995, **117**, 8232–8242.
35 D. Enders and U. Kallfass, *Angew. Chem., Int. Ed.*, 2002, **41**, 1743–1745.